Processing and Application of Ceramics 11 [1] (2017) 13–20
DOI: 10.2298/PAC1701013A

Fabrication of porous bioceramics for bone tissue applications using luffa cylindrical fibres (LCF) as template

Mazen Alshaaer[1,2,*], Mohammed H. Kailani[3], Nidaa Ababneh[4], Saida A. Abu Mallouh[5], Bassam Sweileh[3], Abdalla Awidi[4]

[1]*Plasma Technology and Material Science Unit (PTMSU), Department of Physics, College of Science and Humanitarian Studies, Prince Sattam Bin Abdul Aziz University, 11942 Alkharj, Saudi Arabia*
[2]*Geobiosciences, Geotechnologies and Geoengineering Research Center, University of Aveiro, Campus de Santiago, 3810-193, Aveiro, Portugal*
[3]*Department of Chemistry, The University of Jordan, Amman 11942, Jordan*
[4]*Cell Therapy Center (CTC), The University of Jordan, Amman 11942, Jordan*
[5]*Hamdi Mango Center for Scientific Research, The University of Jordan, Amman 11942, Jordan*

Received 5 October 2016; Received in revised form 29 November 2016; Accepted 2 February 2017

Abstract

Three-dimensionally ordered macroporous biomaterials containing hydroxyapatite were synthesized using natural luffa cylindrical fibres (with diameter of 100–400 μm) as templates. The preliminary evaluation of this novel method for production of porous bioceramics showed promising potential applications in bone tissue engineering. The produced bioceramics were subjected to microstructural, physical, mechanical, and in vitro characterisation. Mercury intrusion porosimetry, supported by SEM analysis, showed the presence of bimodal porosity (smaller pores with diameters of 10 to 30 μm and cylindrical macropores with diameters from 100 to 400 μm) and 60% of the interconnected porosity. These porous calcium phosphate ceramics proved to be bioactive and exhibited mechanical properties comparable to those of natural spongy bones with compressive strength up to 3 MPa and elastic modulus in compression around 0.05 GPa. In vitro characterization of the porous ceramics showed cells attaching to the apatite crystals that make up the scaffold matrix. Cell adhesion resulted in elongated and highly stretched cells within the macropores with focal adhesion points on the scaffolds. Moreover, the cells adhered to the calcium phosphate cement (CPC) and developed cytoplasmic extensions as shown by SEM imagery. Their proliferation in the scaffolds in culture demonstrates that the scaffold architecture is suitable for Mesenchymal stem cells seeding and growth.

Keywords: *calcium phosphate, bioceramics, porous materials, hydroxyapatite, young modulus*

I. Introduction

The design and synthesis of scaffolds as cell carriers have become an important research area in bone tissue engineering. These scaffolds must be biocompatible, osteoconductive, osteoinductive and biodegradable, and should moreover have appropriate biomechanical properties prior to the regeneration of the tissue [1,2]. Some of the most promising biomaterials for application in bone tissue engineering are bioceramic-based materials such as hydroxyapatite (HA), calcium phosphate, bioactive glass and composite materials combining bioactive inorganic materials with biodegradable polymers [3–6].

Bioactive inorganic materials are capable of reacting with physiological fluids to form tenacious bonds to bone through the formation of bone-like hydroxyapatite layers, which provide effective biological interaction and fixation of bone tissue with the material surface [5]. It is now widely accepted that to establish a bond with bone, the biologically active mineral surface layer should form at the material/bone interface [6–9]. Previous studies [10] show that three-dimensional (3D) channels embedded into scaffolds play a vital role in cell immobilization, proliferation and nutrient transfer. Ide-

*Corresponding author: tel: +966 594210931,
e-mail: *mazen72@yahoo.com*

ally, the scaffold's 3D channels ensure sufficient nutrient delivery and gas exchange to promote uniform cell attachment and growth [11–16]. The flow channel of an ideal scaffold would have anatomical features suited for the growth and regeneration of the bone.

From a morphological standpoint, scaffolds must feature adequate porosity, having a well-developed network of interconnected pores over 100 μm in order to promote cell penetration, tissue ingrowth and vascularization [15]. Further necessary features are a controlled bioactivity, a bio-resorbability rate compatible with the spontaneous bone regeneration rate, a mechanical behaviour comparable with that of the natural bone, and a porous network suitable for cell penetration, tissue ingrowth and vascularization [17]. Higher pore sizes (>100 μm) are required for enhanced new bone formation, greater bone ingrowth and the development of capillaries. In terms of vascularization, pore size has been appeared to influence the progression of osteogenesis. A fine pore network would favour hypoxic conditions and induce osteochondral formation before osteogenesis, while macro pores that are well-vascularized lead to direct osteogenesis (without preceding cartilage formation) [6]. Yet higher scaffold porosity results in reduced mechanical properties, thus indicating an upper limit for functional pore size and porosity. This means that a balance must be reached depending on the repair rate, remodeling rate and/or rate of degradation of the scaffold material [6]; and the scaffold design calls for optimal porosity enabling sufficiently appropriate permeability (i.e., pore interconnectivity) for waste removal and nutrient supply along with adequate stiffness and strength to sustain the loads transmitted to the scaffold from the surrounding healthy bone [16]. Most studies suggest that a pore distance in the range of 100–400 μm is satisfactory [3], and pores ought to be interconnected.

Mazali and Alves [4] introduced an inorganic replica of the fibrous network of luffa sponge for the production of a porous medium. The authors synthesized HA porous ceramic for different applications, particularly medical ones, and found that the template proposed (luffa cylindrical fibres), allowed for the preparation of inorganic replicas of very desirable size, on the centimeter scale. However, this porous scale is not appropriate for bone tissue engineering [3]. Therefore, our research focuses on using only a homogeneous and symmetrical portion of the luffa cylindrica.

The aim of this contribution is to present a new design of porous calcium phosphate (i.e. hydroxyapatite) ceramics, characterized with bimodal pore structure and open cylindrical macropores, for bone tissue engineering. The CaP phase selected for this work was HA in view for its chemical likeness to bone mineral. The model could be adapted for use with other CaP powders, such as TCP, which offer the advantage of faster dissolution under physiological conditions. The fabrication of these porous bioceramics was based on sintering calcium phosphate cement coated on luffa cylindrical fibres (LCF). The sponge gourd, the fruit of LCF, has a ligneous netting system in which the fibrous cords are disposed in a multidirectional array, forming a natural mat. The studies by Gianpietro *et al.* [17] and Akhtar *et al.* [18,19] involved LCF composed of 60% cellulose, 30% hemicellulose and 10% lignin. In the present study, the outer core of the network of dried fruits of luffa cylindrical fibres is introduced as a template to produce three-dimensional interconnected porous ceramics with cylindrical pores suitable for bone tissue engineering. The produced scaffolds were evaluated in vitro. The pore size, geometry, and porosity of ceramic scaffolds prepared using this method can be easily controlled by selecting the desired diameter of the LCF, from 100 to 400 μm. The use of this renewable resource material to produce bioceramic scaffolds is spreading worldwide, given its low cost, attractive network structure, and the fibres geometry and range of diameters.

II. Materials and methods

2.1. Fabrication of porous scaffolds

The luffa sponge was obtained from dried fruits of luffa cylindrical fibre (LCF). Only the outer core was used as the replica to obtain the desired pore size (100–400 μm). The homogeneous outer core of the sponge was cut into discs with diameter of 20 mm and thickness of 5 mm, which were then washed in warm water several times. The luffa discs were immersed in sodium hydroxide solution (2 M) for 2 h at 120 °C to remove the waxy and gummy content [19]. The obtained fibre discs were washed with distilled water and dried at 80 °C during 24 h. Fine dried wood chips (bulk density 0.38 g/cm^3) with sizes from 100 to 400 μm were prepared and mixed with the luffa fibres to obtain the 3D structure.

The tetra calcium phosphate (TTCP) powder was prepared from the reaction of dicalcium pyrophosphate ($Ca_2P_2O_7$) (Merck, Germany) and calcium carbonate ($CaCO_3$) (Merck, Germany) with a weight ratio of 1 : 1.27 [17,20,21]. Dicalcium pyrophosphate and calcium carbonate powders were mixed and ball milled for one hour without applying too much force. The powders were then heated at 1500 °C in a box furnace for 1 h and then the red-hot alumina boat containing the powder was taken out and immediately placed into a desiccator and covered until it reached room temperature. The obtained powder (TTCP) was only lightly ground and homogenized in an agate mortar for few minutes.

The TTCP powder was mixed with luffa fibres (luffa fibre/TTCP weight ratio of 0.05) and with wood chip fibres (wood chip/TTCP weight ratio of 0.17) to obtain CPC (calcium phosphate cement) powder. The CPC powder was then blended with diammonium hydrogenphosphate ($(NH_4)_2HPO_4$, 33.3 wt.%) hardening solution with TTCP concentration of 0.34 ml/g. The hardened CPC was removed from the mold and immersed into Hanks' physiological solution at 37 °C for 2 days to increase its strength. Afterward, the scaffolds were fired

at 1100 °C for 2 h, with a heating and then cooling rate of 3 °C/min to remove the luffa fibres and wood chips.

2.2. Characterization of scaffolds

Scanning electron microscope, SEM (Inspect F50, FEI, USA) was used to examine the specimens. The Mesenchymal stem cells (MSCs) attached to the scaffolds were rinsed twice with 2 ml of 1X PBS and fixed with 2% gluteraldehyde for one day at 4 °C. The scaffolds were then subjected to graded alcohol dehydrations, and they were air dried using filter papers, then sputter-coated with platinum. Matrices without cells were used as controls.

X-ray diffraction (XRD) was used to identify the microstructural phases of the reaction products such as the TTCP powder, the set CPC and the sintered CPC. Before the XRD analysis, the samples were ground into fine powders and each powder was put in a specimen holder for the diffractometer (Shimadzu XRD-6000 using CuKα radiation at 20 mA, 40 kV, Japan). Scans were performed from 5° to 80° at a rate of 2°/min.

Pore structure of the scaffolds (1–400 μm) was determined by mercury intrusion porosimetry (PoreMaster, USA), i.e. differential mercury intrusion volume related to the applied pressure. The scaffolds were placed in a closed cell (Penetrometer) and evacuated. The total porosity (*TP*) of the scaffold was determined from bulk density (ρ_B) (ration between sample weight and volume) and skeletal density for solid fraction (ρ_0) obtained by Helium-pycnometry:

$$TP = 100 \cdot \left(1 - \frac{\rho_B}{\rho_0}\right) \tag{1}$$

The dimensions and the weight of each scaffold were measured and recorded through a Vernier caliper and an electronic balance, respectively.

The compressive strength of the scaffold was measured using rubber pads placed on the top and the bottom surfaces of each scaffold [21]. The rubber-padded scaffold was then placed in a CBR tester (CONTROLS, Italy) to conduct a compressive test. The rubber pads were used to ensure a uniform distribution of the applied load onto the sample. A crosshead speed of 0.2 mm/min was used for the compressive tests. The material's stress-strain curve shows a linear region where the material follows Hooke's Law. Hence, for this region:

$$\sigma = E \cdot \varepsilon \tag{2}$$

where E refers to Young's modulus for compression, and ε is the strain caused by the compressive stress.

2.3. In vitro characterization of scaffolds

MSC Cell Isolation – MSCs were isolated from human bone marrow aspirates via density gradient centrifugation. The cells were expanded in non-differentiating MSC growth medium (CCM) consisting of α-minimal essential medium (α-MEM), with 10% fetal bovine serum (FBS), 1% penicillin-streptomycin (PEN-STREP) and 2 mM glutamine. The cells were incubated at 37 °C with 5% CO_2. After they reached 90% confluence, the cells were harvested by rinsing with 0.25% trypsin and 0.03% EDTA solution; they were expanded into a second passage until they reached 80% confluence, and then trypsinized and cryopreserved in liquid nitrogen. These cells were designated as passage 1 (P1) cells.

Osteogenic Differentiation – The cells were seeded in 12 multi-well plates for an estimated 80% confluence. Each experiment comprised 12 cultures – 6 under osteogenic conditions and 6 controls under normal cell culture conditions (CCM). To induce the osteogenic differentiation of the MSCs, the cultures were maintained in osteogenic media consisting of 60 μM ascorbic acid, 10 mM β-glycerol phosphate and 100 nM dexamethasone. The medium was changed every 2–3 days. After 21 days of differentiation experiments, with and without osteogenic media, the cells were evaluated via Alizarin Red Staining (ARS) and silver nitrate.

Cell Seeding on the Scaffolds – Cryopreserved (P1) cells were re-plated at a seeding density of 4000 cells/cm^2 in alpha MEM as described above. At near confluency, P2 cells were harvested with 0.25% trypsin in EDTA and resuspended at a density of 2×10^5 cells/ml alpha-MEM plus 1% penicillin/streptomycin. The calcium phosphate scaffolds were sterilized in 70% ethanol for 24 h and then incubated with cell culture media containing 10% FBS for at least 4 h. The MSCs were seeded into the scaffolds with a cell seeding density of 200 000

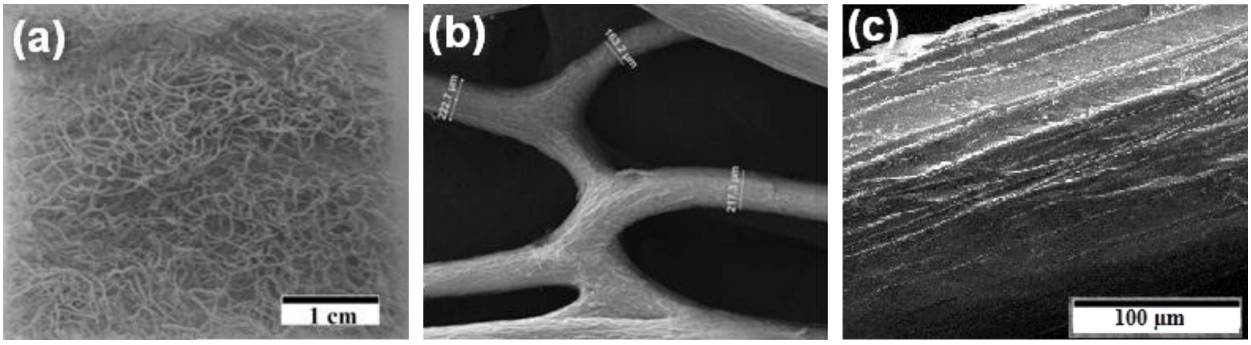

Figure 1. SEM micrographs of treated luffa fibres: a) treated luffa fibre mat, b) fibre network and c) surface morphology of luffa fibres

cells/per scaffold. The MSCs were cultured with osteogenic medium and cell culture medium as a standard control to verify their proliferative and differentiation potential at 37 °C and 5% CO_2 for 4 weeks. The media was changed every 3–4 days.

III. Results and discussion

3.1. Structure of porous calcium phosphate scaffold

The homogenous treated outer cores of luffa cylindrical fibres (Fig. 1a) are well connected and have diameters around 100 to 400 μm (Fig. 1). These sizes and the connected fibre structure are within the requirements [16] for use as a template for the interconnected macropores of the bioceramic scaffold. As can be seen in Fig. 1c, the natural fibres are cylindrical and have rough surfaces. The large spaces between the fibres were filled with wood chips to increase the overall macroporosity, and to extend the luffa mat into a three dimensional structure.

When the luffa sponge was submerged in the CPC slurry, the calcium phosphate particles carried by the aqueous solution were able to coat the luffa fibres and the embedded wood chips. Since the CPC slurry was made of TTCP powder plus the $(NH_4)_2HPO_4$ solution, the coating process was completed before the start of the setting reaction (i.e. the reaction between TTCP and Na_2HPO_4 solution to form poorly crystallized hydroxyapatite). The LCF and wood chips coated with CPC were left at 37 °C under hydrothermal conditions for 1 h. After the setting reaction, the slurry-coated LFC was dried in the air at room temperature. The setting reaction to form the hydroxyapatite phase made the CPC framework strong enough to stand freely, without sagging or distortion due to weight. Previous studies [4] report that a full decomposition and evaporation of LCF take place around 600 °C, leaving a pure inorganic matrix. The degradation reactions and evaporation of the LFC components take place under the sintering temperature [4]. Therefore this material will not have any influence on the biological properties of the end products.

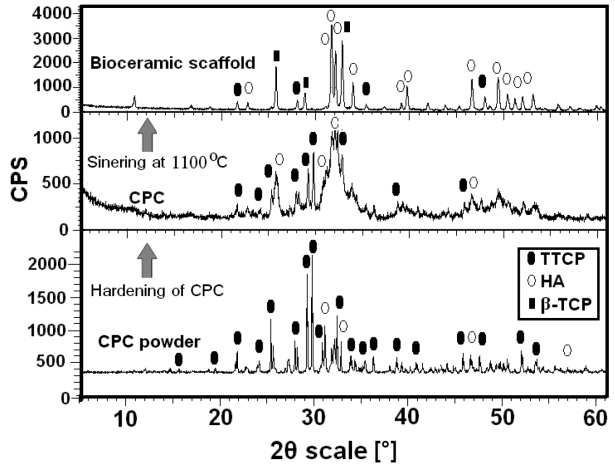

Figure 2. XRD patterns of CPC powder, sintered CPC and sintered porous calcium phosphate sample (scaffold)

The XRD analysis (Fig. 2) revealed that TTCP is formed as the main phase in the CPC powder through heating the mixture of pyro-calcium phosphate ($Ca_2P_2O_7$) and calcium carbonate ($CaCO_3$) at 1500 °C for 5 h, followed by quenching in air. Moreover, this CPC powder contained a few peaks corresponding to HA. The peaks are strong and sharp, indicating a relatively high crystallinity of the powder.

After hardening the CPC sample contains the hydroxyapatite phase (Fig. 2) in the form of HA nano-crystals (Fig. 3a), but some residual TTCP were still left behind (Fig. 2). In addition, the residual TTCP phase was depleted to a great extent due to the formation of hydroxyapatite. The high backgrounds of the middle XRD pattern (Fig. 2) at 30–35° and 45–55° indicate the presence of amorphous or poorly crystalline CaP phase, mainly CDHA (calcium-deficient HA) as shown by the EDS measurements with a Ca/P ratio of 1.6. High crystalline stoichiometric HA exhibit low solubility in water or body fluids whereas CDHA are more soluble [1]. Therefore the CDHA is more soluble and more efficient in inducing bone like apatite than HA.

Upon sintering the scaffold at 1100 °C for 2 h, there was a dramatic change in the calcium phosphate grain

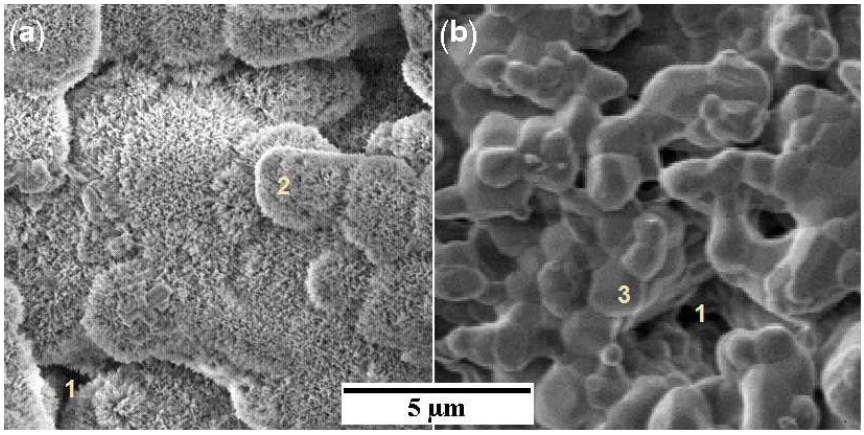

Figure 3. SEM images of: a) CPC surface after immersion for 2 days in SBF and b) sintered hydroxyapatite at 1100 °C (1: pores, 2: nano size hydroxyapatite layers, 3: hydroxyapatite grains)

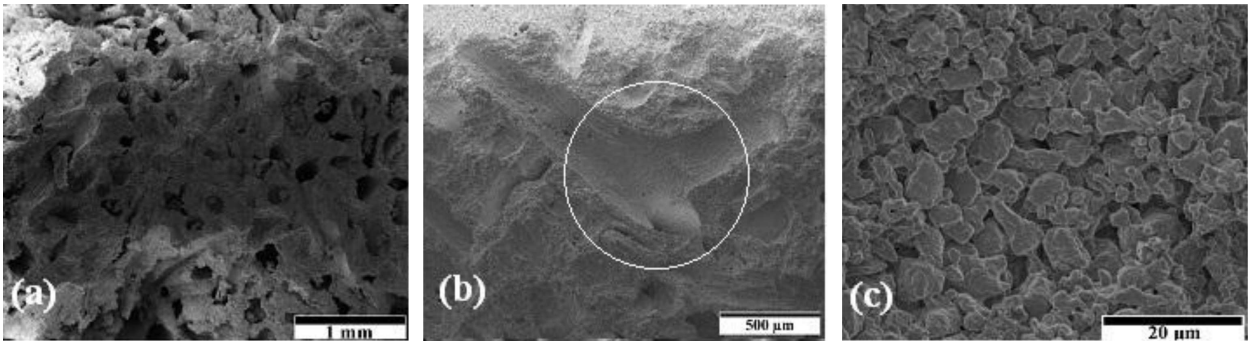

Figure 4. SEM micrographs of fracture surface of the sintered porous calcium phosphate. Evaluation of porosity and LCF-like flow channel network along a cross-section (a), a longitudinal section (b) and pore structure of the porous scaffold (c)

morphology due to the grain growth (Fig. 3). During sintering the cement particles were joined together, but the CPC framework was not damaged by thermal removal of the LCF and WS at 1100 °C (Fig. 3b). Nevertheless, after sintering at 1100 °C for 2 h, equal-axed hydroxyapatite grains were formed even though macropores remained in the structures (Fig. 3b). In addition to the hydroxyapatite and the residual TTCP, some β-TCP was found in the sintered CPC at 1100 °C indicating a certain degree of thermal decomposition of the hydroxyapatite phase into the tricalcium phosphate phase (Fig. 2). However, all these phases are a group of reactive biomaterials.

3.2. Morphological and mechanical characterization

Porous calcium phosphate ceramic with a LCF-like structure was prepared by heating at 1100 °C which resulted in burn out of the LCF template and consolidation of the calcium phosphates. The products exhibit porous structures corresponding to negative replication of LCF and wood chips. The fabricated scaffold with a LCF-like flow channel network is shown in Fig. 4a. Another feature of the sintered porous CPC was the presence of well-connected cylindrical channels, with diameters between 100 and 400 µm inside the struts. Morphological analysis on cross- and longitudinal-sections of these LCF-like channels is presented in Fig.4b. The sintered porous CPC contained mainly hydroxyapatite phase with macropores (as a replica of the wood chips and fibres in the LCF) in the overall structure, and smaller open pores in the struts. This design of bioceramic scaffolds with well-connected cylindrical channels, or highly effective porosity, is intended to favour an increase in the mass transport of nutrients and oxygen, as well as enhance removal of waste products for cell growth.

Pore interconnectivity first arises through the connected LCF mat and the contact point between adjacent grains (Fig. 4b), yet also due to the presence of smaller pores (up to 30 µm) induced by the phase conversion mechanism [22]. The macropore network within these channel walls can be observed in Fig. 4c. The cross-section image in Fig. 4b reveals a continuous LFC-like channel within the scaffold.

To confirm the qualitative morphological evaluation performed by SEM, a quantitative estimation of porosity characteristics was performed by mercury intrusion porosimetry (MIP). As can be seen in Fig. 5, MIP shows a bimodal distribution of pore size, characterized by pores of a few micrometers in diameter along with macropores of the order of hundreds of micrometers. It is apparent that the total open pore volume is nearly 60% of the scaffold volume (Fig. 5a). The calculations and measurements of volume, weight, and bulk density indicate a total porosity around 61%. The skeletal density, determined by helium pycnometer, is around 3.162 g/cm^3. Thus, around 97% of the pores are connected [27,28]. The porosity consists of the smaller pores (33%), with diameters ranging from 10 to 30 µm and larger pores, ranging from 100 to 400 µm (50%). In

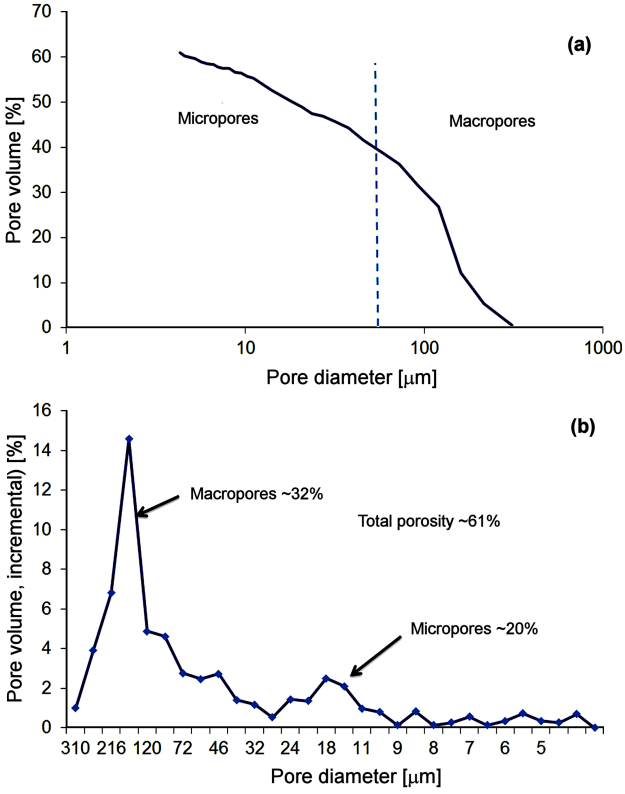

Figure 5. Mercury intrusion porosimetry of bioceramic scaffold: a) cumulative pore size distribution and b) incremental pore size

Table 1. Comparison of the bioceramic scaffold and cancellous bones [21,25,26]

Materials	Compressive strength [MPa]	Total porosity [%]	Bulk density [g/cm^3]	Macropore size [μm]	Elastic modulus [GPa]
Bioceramic scaffold	3	62	1.21	100–400	0.05
Cancellous bones	0.2–80	30–90	1-1.4	200–400	0.01–2

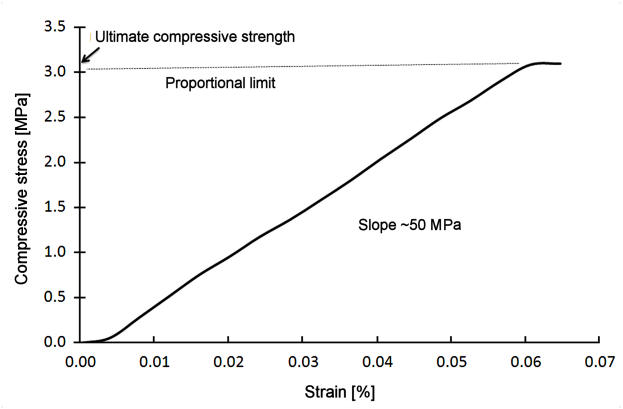

Figure 6. Representative linear part of stress-strain responses to the compression test of scaffold

this structure, the large macropores are suitable for the accommodation of osteoblast and undifferentiated bone mesenchymal stem cells, while the smaller pores serve as interconnection bridges between adjacent macropores, able to promote nutrient and metabolite exchange [23,24], thus improving the structural interconnectivity.

One of the most important requirements of an ideal bone substitute is mechanical behaviour matching that of the bone tissue to be restored. An accurate mimesis of specific mechanical properties, such as the elastic modulus, may be crucial for an effective reproduction of the functional response of natural tissue, especially in load-bearing applications. In the past decade, the use of polymers such as PLA, PGA and PCL has become a popular strategy for the provision of biodegradable supports for orthopedic applications [17]. However, their deficient mechanical properties limit their use, mainly to a restricted number of non-load-bearing applications [22].

Figure 6 shows the representative linear part of stress-strain response of the fabricated bioceramic scaffold. This diagram shows that the scaffold exhibits a compressive strength of 3 MPa. The elastic modulus of the scaffold in compression, ~50 MPa, was obtained from the slope of the stress-strain curve. The bulk density of the scaffold is 1.21 g/cm^3, and the total porosity is 62%. Because the mechanical and physical properties of the scaffold lie within the range of those of cancellous bone, as shown in Table 1, this can be considered a promising scaffold material for hard tissue regeneration.

3.3. Preliminary evaluation of biocompatibility of scaffolds

The bioceramic scaffolds were prepared for *in vitro* cultivation. Mesenchymal stem cells (MSCs) were seeded on the 3D scaffolds and maintained with osteogenic medium for 1 month. After 1 month, most pores were filled with new tissue mass, as observed by SEM. The HA matrices visually demonstrated high cell density on the surfaces of the matrix within the cylindrical macropores as seen in Figs. 7a and 7b.

Figures 8a and 8b show cells attached to the apatite crystals that make up the scaffold matrix. Cell adhesion resulted in elongated and highly stretched cells within the macropores, with focal adhesion points on the scaffolds (Fig. 9). Moreover, the cells adhered to the CPC and developed cytoplasmic extensions, visible in Fig. 9, with a proliferation in the culture demonstrating that the scaffold architecture was suitable for MSC seeding and growth. The increased porosity and interpore connectivity of the biomaterial give rise to high density and multiple layers of cells. The newly forming bone tissue follows the outline of the bioactive HA surface (Fig. 9), while the bone matrix consists of hydroxyapatite crys-

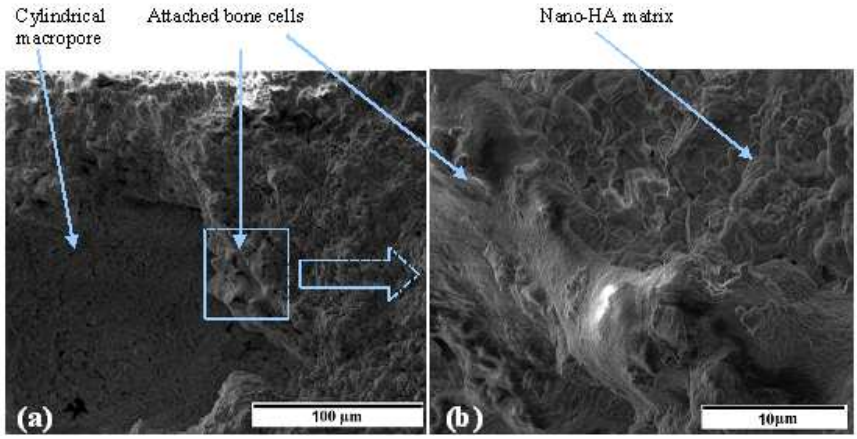

Figure 7. SEM of bone cells and tissues present within the cylindrical macropores of the scaffold: a) low magnification and b) enlarged insert

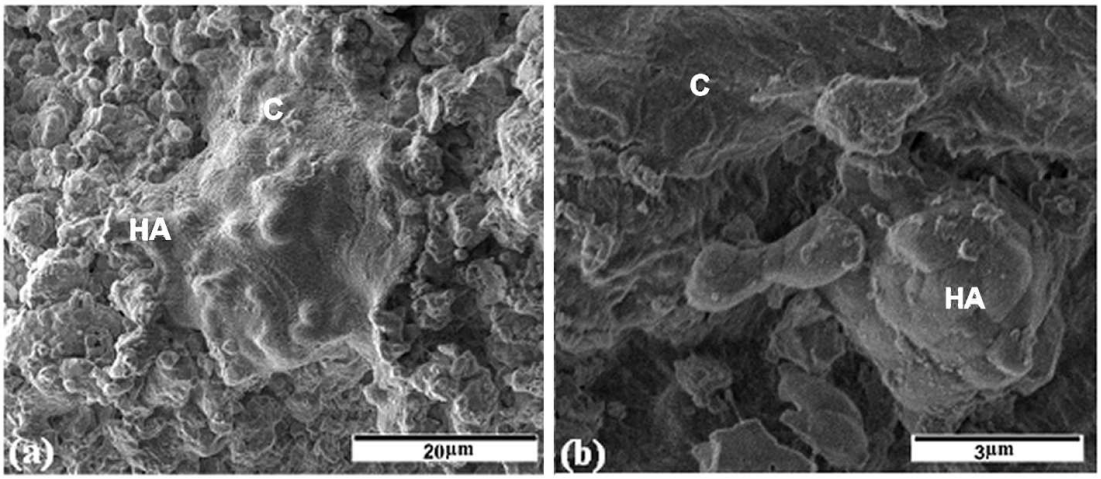

Figure 8. SEM micrographs showing: a) osteoblast cell attached to the surface of the bioceramic scaffold and b) the cell attaching to the apatite crystals that make up the bioceramic matrix (C: cell, HA: hydroxyapatite matrix)

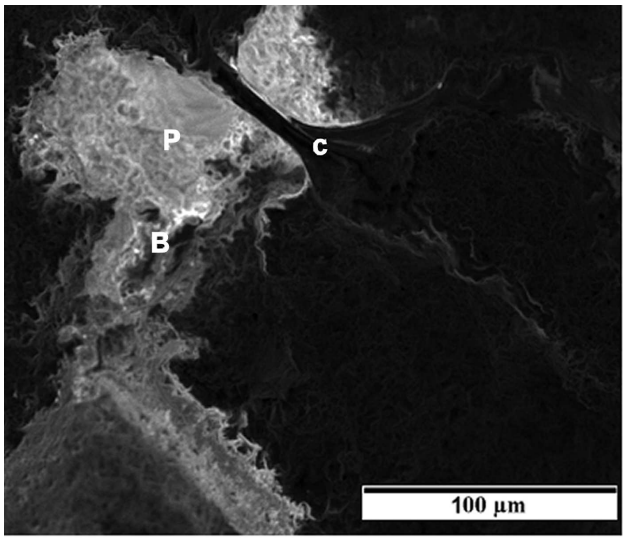

Figure 9. Formation of new bone tissue, as the cellular processes extend over the underlying scaffold matrix with cytoplasmic extensions (C: cytoplasmic extension, P: macropore, B: new bone tissues and minerals)

tals containing calcium and phosphorus. These factors provide important indications of osteogenic differentiation.

IV. Conclusions

The present study introduces a new methodology for preparing porous calcium phosphate ceramics for bone tissue engineering. We developed a degradable porous scaffold, prepared using the homogeneous outer core of luffa cylindrical fibre (LCF) as the replication method. The advantage of the method was the attainment of high pore interconnectivity with acceptable mechanical properties. The resulting bioceramic material, with its novel bimodal pore structure, represents a valid means of achieving adequate porosity requirements while providing adequate support in load-bearing applications.

This proposal for preparing porous bioceramic scaffolds is as quick and versatile as conventional technologies. The method produced porous hydroxyapatite-based calcium phosphate ceramics with bimodal pore structure (consisting of macropores ranging from 100 to 400 μm and smaller pores with diemeter 10 to 30 μm), and 60% of open porosity. The preliminary *in vitro* characterization demonstrates the formation of new bone tissue, as the cellular processes extend over the underlying scaffold matrix with cytoplasmic extensions. In this structure, the macropores are suitable for the accommodation of osteoblast and undifferentiated bone mesenchymal stem cells, while the smaller pores serve as interconnection bridges between adjacent macropores, able to promote nutrient and metabolite exchange, thus improving the structural interconnectivity. The elastic modulus of the scaffold in compression is ~50 MPa, and the bulk density of the scaffold is 1.21 g/cm^3. Because the mechanical and physical properties of the scaffold lie within the range of those of cancellous bone, this can be considered as a promising scaffold material for hard tissue regeneration.

The *in vitro* investigations reported that cells attached to the apatite crystals that make up the scaffold matrix. Moreover, the cells adhered to the CPC and developed cytoplasmic extensions, demonstrating that the scaffold architecture was suitable for MSC seeding and growth. These factors provide important indications of osteogenic differentiation.

Acknowledgements: Financial support for the project, grant no. 1442, "Synthesis and characterization of scaffolds for bone tissue engineering" provided by the Deanship of Academic Research at the University of Jordan is gratefully acknowledged. We would like to take this opportunity to thank Hamdi Mango Center for Scientific Research (HMCSR), University of Jordan for the use of their laboratory facilities.

References

1. R. Ghosh, R. Sarkar, S. Paul, "Development of machinable hydroxyapatite-lanthanum phosphate composite for

biomedical applications", *Mater. Design*, **106** (2016) 161–169.
2. L.L. Hench, J.M. Polak, "Third-generation biomedical materials", *Science*, **295** (2002) 1014–1017.
3. L. Gerhardt, A.R. Boccaccini, "Bioactive glass and glass-ceramic scaffolds for bone tissue engineering", *Materials*, **3** (2010) 3867–3910.
4. I.O. Mazali, O.L. Alves, "Morphosynthesis: high fidelity inorganic replica of the fibrous network of loofa sponge (Luffa cylindrica)", *An. Acad. Bras. Cienc.*, **77** [1] (2005) 25–31.
5. Z. Sheikh, Y.L. Zhang, L. Grover, G.E. Merle, F. Tamimi, J. Barralet, "In vitro degradation and in vivo resorption of dicalcium phosphate cement based grafts", *Acta Biomater.*, **26** (2015) 338–346.
6. J. Zhang, W. Liu, V. Schnitzler, F. Tancret, J. Bouler, "Calcium phosphate cements for bone substitution: Chemistry, handling and mechanical properties", *Acta Biomater.*, **10** (2014) 1035–1049.
7. C. Bergemann, M. Cornelsen, A. Quade, T. Laube, M. Schnabelrauch, H. Rebl, V. Weißmann, H. Seitz, B. Nebe, "Continuous cellularization of calcium phosphate hybrid scaffolds induced by plasma polymer activation", *Mater. Sci. Eng. C*, **59** (2016) 514–523.
8. X. Wang, W. Li, "Biodegradable mesoporous bioactive glass nanospheres for drug delivery and bone tissue regeneration", *Nanotechnol.*, **2016** [22] (2016) 225102.
9. X. Shanglong, L. Dichen, L. Bingheng, T. Yiping, W. Chaofeng, W. Zhen, "Fabrication of a calcium phosphate scaffold with a three dimensional channel network and its application to perfusion culture of stem cells", *Rapid Prototyping J.*, **13** [2] (2007) 99–106.
10. J.C. Almeida, A. Wacha, P.S. Gomes, L.C. Alves, M.H.V. Fernandes, I.M.M. Salvado, M.H.R. Fernandes. "A biocompatible hybrid material with simultaneous calcium and strontium release capability for bonetissue repair", *Mater. Sci. Eng. C*, **62** (2016) 429–438.
11. I. Ochoa, J.A. Sanz-Herrera, J.M. García-Aznar, M. Doblaré, D.M. Yunos, A.R. Boccaccini, "Permeability evaluation of 45S5 Bioglass®-based scaffolds for bone tissue engineering", *J. Biomech.*, **42** (2009) 257–260.
12. M. Alshaaer, M.H. Kailani, H. Jafar, N. Ababneh, A. Awidi, "Physicochemical and microstructural characterization of injectable load-bearing calcium phosphate scaffold", *Adv. Mater. Sci. Eng.*, **2013** (2013) 149261.
13. H. Zhou, J.G. Lawrence, S.B. Bhaduri, "Fabrication aspects of PLA–CaP/PLGA–CaP composites for orthopedic applications: A review", *Acta Biomater.*, **8** (2012) 1999–2016.
14. F. Tamimi, D. Le Nihouannen, H. Eimar, Z. Sheikh, S. Komarova, J. Barralet, "The effect of autoclaving on the physical and biological properties of dicalcium phosphate dihydrate bioceramics: Brushite vs. monetite", *Acta Biomater.*, **8** (2012) 3161–3169.
15. W. Liu, J. Zhang, G. Rethore, K. Khairoun, P. Pilet, F. Tancret, J. Bouler, P. Weiss, "A novel injectable, cohesive and toughened Si-HPMC (silanized-hydroxypropyl methylcellulose) composite calcium phosphate cement for bone substitution", *Acta Biomater.*, **10** (2014) 3335–3345.
16. R.M. Pilliar, R.A. Kandel, M.D. Grynpas, J. Theodoropoulos, Y. Hu, B. Allo, A. Changoor, "Calcium polyphosphate particulates for bone void filler applications", *Biomed. Mater. Res. B: Appl. Biomater.*, (2016) http://dx.doi.org/10.1002/jbm.b.33623
17. K. Genovese, "Three-dimensional microscopic deformation measurements on cellular solids", *J. Mech. Behavior Biomed. Mater.*, **60** (2016) 78–92.
18. N. Akhtar, A. Saeed, M. Iqbal, "Chlorella sorokiniana immobilized on the biomatrix of vegetable sponge of Luffa cylindrica: A new system to remove cadmium from contaminated aqueous medium", *Bioresour. Technol.*, **88** [2] (2003) 163–165.
19. O.A. Valcineide, H.D. Tanobea, M.M. Sydenstrickera, S.C. Amicoa, "A comprehensive characterization of chemically treated Brazilian sponge-gourds (Luffa cylindrica)", *Polymer Testing*, **24** (2005) 474–482.
20. Z. Sheikh, M. Geffers, T. Christel, J. Barralet, U. Gbureck, "Chelate setting of alkali ion substituted calcium phosphates", *Ceram. Int.*, **41** (2015) 10010–10017.
21. V. Guarino, L. Ambrosio, "The synergic effect of polylactide fiber and calcium phosphate particle reinforcement in poly e-caprolactone-based composite scaffolds", *Acta Biomater.*, **4** (2008) 1778–1787.
22. N. Lertcumfua, P. Jaitaa, S. Manothama, P. Jarupoomd, S. Eitssayeama, K. Pengpata, G. Rujijanagula, "Properties of calcium phosphates ceramic composites derived from natural materials", *Ceram. Int.*, **42** [9] (2016) 10638–10644.
23. K.J.L. Burg, S. Porter, J.F. Kellam, "Biomaterial developments for bone tissue engineering", *Biomaterials*, **21** (2000) 2347–2359.
24. H. Zhou, S. Kong, Z. Liu, Y. Pan, Y. Liu, M. Luo, L. Deng, "Fabrication and evaluation of calcium alginate/calcium polyphosphate composite", *Mater. Lett.*, **180** (2016) 184–187.
25. J. Russias, E. Saiz, R.K. Nalla, K. Gryn, R.O. Ritchie, A.P. Tomsia, "Fabrication and mechanical properties of PLA/HA composites: a study of in vitro degradation", *Mater. Sci. Eng. C*, **26** (2006) 1289–1295.
26. Y. Li, H. Zuo, Y. Guo, T. Miao, Q. Pan, "Renewable lignosulfonate-assisted synthesis of hierarchical nanoflake-array-flower ZnO nanomaterials in mixed solvents and their photocatalytic performance", *Nanoscale Res. Lett.*, **11** (2016) 260.
27. M. Alshaaer, H. Cuypers, H. Rahier, J. Wastiels, "Production of monetite-based inorganic phosphate cement (MIPC) using hydrothermal post curing (HTPC)", *Cement Concrete Res.*, **41** [1] (2011) 30–37.
28. M. Alshaaer, H. Cuypers, G. Mosselmans, H. Rahier, J. Wastiels, "Evaluation of a low temperature hardening inorganic phosphate cement for high-temperature applications", *Cement Concrete Res.*, **41** [1] (2011) 38–45.